Bandgap-confined large-mode waveguides for surface plasmon-polaritons

Carsten Reinhardt,[1,*] Andrey B. Evlyukhin,[1] Wei Cheng,[1] Tobias Birr,[1] Andrey Markov,[2] Bora Ung,[2] Maksim Skorobogatiy,[2] and Boris N. Chichkov[1]

[1]*Laser Zentrum Hannover e.V., Hollerithallee 8, D-30419 Hannover, Germany*
[2]*Department of Engineering Physics, Ecole Polytechnique de Montréal, C.P 6079, succ. Centre-Ville, Montreal, Quebec H3C 3A7, Canada*
**Corresponding author: c.reinhardt@lzh.de*

Received July 9, 2013; revised September 10, 2013; accepted September 13, 2013; posted September 16, 2013 (Doc. ID 193632); published October 15, 2013

The optical properties of a novel type of open waveguiding structure for surface plasmon-polaritons (SPPs) are experimentally investigated. The waveguide consists of a strip-like region of a gold surface confined by a periodic sequence of dielectric ridges forming a Bragg-type reflector. This bandgap structure resembles the plasmonic analogue of an antiresonant reflecting optical waveguide (ARROW) for SPPs, providing direct access to the guided plasmonic field. The main structural parameters are evaluated by numerical modeling using the finite element and finite-difference time-domain methods. We investigate field distributions of the plasmonic modes in the antiresonant Bragg-reflector waveguides with varied numbers of dielectric ridges and demonstrate a large mode-area single-mode performance at a telecom wavelength of 1550 nm. Furthermore, for an excitation wavelength of 974 nm, it is shown that different low-order modes can be selectively excited using multiple laser beams with variable phase relation. Selective excitation of single longitudinal and transversal modes of the waveguide is realized by coherent two-beam excitation. Possible sensing applications of these large-mode open waveguides are discussed.

OCIS codes: (240.6680) Surface plasmons; (240.6690) Surface waves; (130.2790) Guided waves; (130.3120) Integrated optics devices.
http://dx.doi.org/10.1364/JOSAB.30.002898

1. INTRODUCTION

The properties and features of surface plasmon-polaritons (SPPs) in different micro- and nanostructured systems have intensively been studied in the last decade [1–3]. Because of the exponential localization of these electromagnetic waves at the interface of a metal with negative permittivity and a dielectric, SPPs have high sensitivity to surface inhomogeneities and optical properties of the surrounding medium. They constitute a unique tool for the realization of novel planar optical devices and sensors operating at the microscale level. A number of micro-optical devices, such as mirrors, lenses, beam splitters, and interferometers for SPPs have been recently demonstrated [4–9].

Various approaches to achieve effective local excitation [10–13] and confined SPP guiding for data transport applications using channel plasmon-polaritons [7,14], metal-insulator-metal structures [15], metal strips and nanowires [16], and dielectrically loaded SPP waveguides (DLSPPWs) [17–24] have been proposed and investigated. These types of SPP waveguides provide a high field confinement down to subwavlength dimensions, making them interesting candidates for an integrated plasmonic circuitry. However, one common drawback of these designs is their intrinsically short propagation length. In contrast to the high confinement schemes are long-range surface plasmon-polaritons (LRSPPs) [25,26]. Their mode confinement is comparable to that of optical fibers, but with LRSPPs' propagation length up to the centimeter range.

An alternative realization of SPP guiding systems is based on the use of nanoparticle chains [27,28] and of periodically structured metal surfaces, exhibiting bandgaps for SPPs [29,30]. If a SPP bandgap (SPPBG) structure provides free narrow spatial channels, i.e., a defect line in the bandgap structure, SPPs can be confined to and guided along these channels with simultaneous access to the guided field, which is important for SPP sensor concepts. Similar guiding effects with respect to SPPs can also be realized using empty channels in random nanoparticle structures [31]. Although the waveguide diameters were in the range of micrometers, and the SPP modes were confined only weakly, the propagation length did not exceed 4–5 μm.

In this article, an alternative and easy-to-fabricate bandgap system for SPP guiding is studied as it is shown in Fig. 1. The waveguiding structure combines the advantage of long propagation lengths with the ability to directly access the plasmonic field. The low mode confinement accompanying the long propagation length is considered advantageous as it allows coupling of the waveguide modes to standard optical fibers. The system under consideration comprises a narrow strip-like region of a metal surface of a few micrometers in width confined by a periodic sequence of dielectric ridges. These periodic ridges constitute a Bragg-type reflector with a photonic bandgap response. SPP waves can thus be confined to the metallic region between the two Bragg reflectors. Due to the reflecting behavior of the SPPBG structure, the waveguide resembles the plasmonic analogue of an

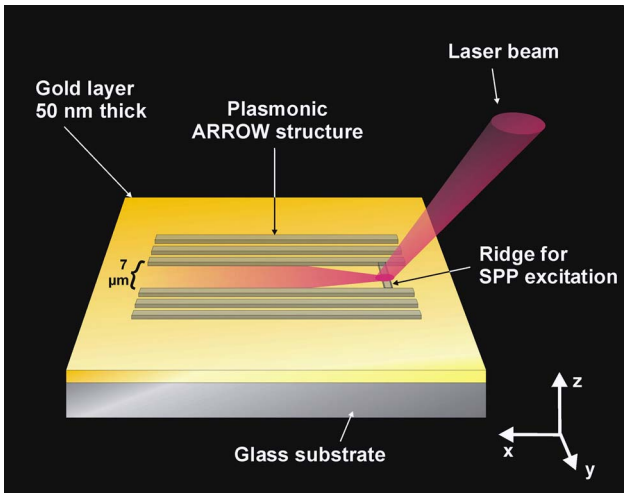

Fig. 1. Schematic of the waveguide layout. SPPs are locally excited by light scattering on a dielectric ridge perpendicular to the waveguide axis. The SPPs are confined by Bragg reflection to the region between the parallel pairs of guiding ridges.

antiresonant-reflecting optical waveguide (ARROW) [32,33]. ARROWs are typically used to propagate light in lower refractive index media compared to the cladding index. This provides the possibility to interferometrically investigate refractive index shifts in gaseous and liquid analytes by accumulating phase shifts of the propagating light wave inside the hollow gas- or liquid-filled core over relatively large distances. Furthermore, these waveguides exhibit large mode areas even for single-mode operation, allowing high optical intensities to be propagated inside the core region [34].

The bandgaps of the waveguiding structure considered in this paper confine locally excited SPPs inside the empty waveguide core region within certain spectral ranges [35]. The guided SPPs can be associated with low-order modes of the corresponding antiresonant reflecting plasmonic waveguide. Although the core diameter is large, the bandgap-confined SPP waveguides have a small number of modes or are even single mode at longer wavelengths, as is shown in the following section. With respect to the large mode area, they are similar to LRSPP waveguides; however, the fields are bounded by the metallic film. The effective refractive index and the propagation length of these modes are strongly sensitive to the wavelength of operation and the waveguide core size, whereas the number of ridges in the periodic reflector is of minor importance. In contrast to LRSPP waveguides, the surface plasmon (SP) ARROW provides an open core and allows direct access to the plasmonic field.

Predominantly, the effective index of the guided SPPs is sensitive to environmental influences, e.g., refractive index changes of the medium above the metallic layer or selective conjunction of the metal surface with molecules, making it attractive for integrated sensor applications using interferometric waveguiding structures for SPPs, for optical characterization of thin metal films, and study of interactions of plane SPP waves with surface nanostructures. The large mode operation may allow direct fiber coupling of the investigated waveguides.

For an experimental realization of the suggested system, the ridges are fabricated by direct laser-writing in spin-coatable epoxy-based resist on a gold-covered glass slide [23]. In this paper, the guiding properties of these new types of waveguides are experimentally investigated and characterized using leakage radiation microscopy (LRM) [18,20–24]. SPP guiding is studied for excitation wavelengths of 1550 and 974 nm in 7 μm wide waveguides, where both wavelengths are confined in the SPPBG. The number of guided SPP modes varies from 1 mode at 1550 nm to two modes at 974 nm. Maximum propagation lengths of up to 47 μm ($1/e$ intensity decay) have been obtained at 974 nm. The experimental studies of the core modes by LRM are supported numerically by the finite element method (FEM) for calculating the waveguide mode structures and the finite-difference time-domain (FDTD) method for simulating the SPP propagation inside the waveguide structure.

Besides excitation of SPP modes in the core with a single beam, the interference between multiple coherent SPP beams with an adjustable phase difference is investigated. Selective excitation of distinct longitudinal modes of the waveguide is realized using two coherent laser beams. It is further demonstrated that the propagating SPP modes inside the SP-ARROW can also be used to realize novel integrated sensor concepts.

2. CALCULATED MODE STRUCTURE

The theoretical principles of bandgap-confined SPP waveguides have been studied in a recent publication [35]. The optical properties of the bandgap plasmonic waveguide are calculated numerically using FEM, as it is implemented in the software package FemSim from RSoft [36]. Note that this simulation does not include SPP losses due to leakage radiation. The material distribution for modeling the electric field component E_z perpendicular to the metal surface and the effective complex mode indices $n = n' + i\kappa$ of the waveguiding structure correspond to the structure shown in Fig. 1. From the complex mode index, the propagation length is calculated according to $L_{\mathrm{spp}} = 1/2k''$, where $k'' = \kappa k_0$ and k_0 is the modulus of the vacuum wave vector of the incident laser light. The Bragg reflectors enclose a 7 μm wide region on a plane gold film of 50 nm thickness. The reflectors consist of up to three dielectric ridges with a width of 650 nm and a height of 500 nm made from polymer with a refractive index of 1.5 separated by a period of 1.5 μm. SPPs inside the waveguide are locally excited by light scattering on an additional thin ridge perpendicular to the optical axis.

Depending on the wavelength, different numbers of modes can be excited in this structure. A FEM numerical simulation for the excitation wavelength of 1550 nm shows one mode with a real part of the mode index of $n'_{1550} = 1.001$ and an imaginary part of $\kappa_{1550} = 0.007$, corresponding to a propagation length of 123 μm. The distribution of the electric field component perpendicular to the metal surface of this mode is shown in Fig. 2. These values are nearly independent on the number of ridges in each Bragg reflector. The mode field diameter is approximately 5 μm, making it attractive for direct coupling to an optical fiber.

For an excitation wavelength of 974 nm, two modes are obtained from the FEM simulations. The fundamental mode with its intensity maximum on the waveguide axis has a real part of the mode index of $n'_{974_0} = 1.007$ and an imaginary part of $\kappa_{974_0} = 0.0007$ [see Fig. 3(a)], resulting in a propagation length of 176 μm. Interestingly, the propagation length in the latter case is longer than that for 1550 nm, which is a consequence

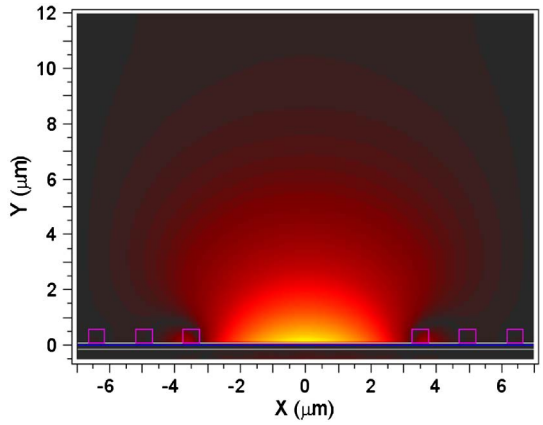

Fig. 2. Mode field distribution of the 7 μm wide plasmonic ARROW at a wavelength of 1550 nm with a real part of the mode index of $n'_{1550} = 1.001$ and an imaginary part of $\kappa_{1550} = 0.007$. The FEM simulation shows single-mode operation with a mode field diameter of about 5 μm. This mode could be efficiently coupled to a fiber mode.

of the field distribution inside the reflector structure, which is extending further into the (assumed) lossless air and polymer regions. Thus, this mode encounters lower absorption, though it sees a slightly higher real refractive index due to the influence of polymer.

The second mode at 974 nm has two maxima with a minimum on the waveguide axis as depicted in Fig. 3(b). The real part of the mode index is $n'_{974_1} = 1.002$, which is lower than

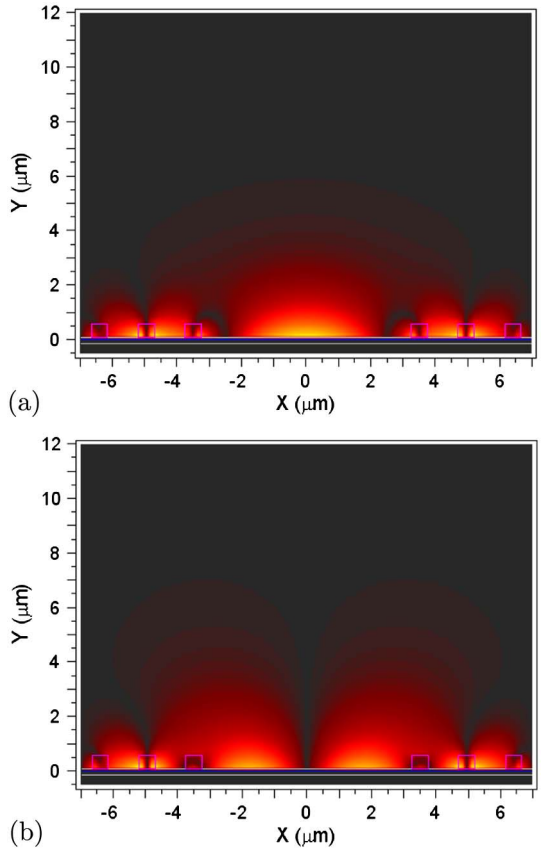

Fig. 3. Mode structure of the 7 μm wide plasmonic ARROW at a wavelength of 974 nm. The structure supports two modes: (a) fundamental mode with $n'_{974_0} = 1.007$ and $\kappa_{974_0} = 0.0007$; (b) first higher-order mode with $n'_{974_1} = 1.002$ and $\kappa_{974_1} = 0.0006$.

the real index of the fundamental mode, since it extends further into the air region. Due to the same reason, the imaginary part of the mode index with a value of $\kappa_{974_1} = 0.0006$ is lower. The propagation length can be calculated to 205 μm.

3. EXPERIMENT

A. Waveguide Fabrication

Direct laser-writing using two-photon polymerization (2PP) is an attractive technology for the fabrication of two- and three-dimensional structures on different substrates with resolutions down to and even less then 100 nm [37]. This approach has previously been demonstrated to be a reliable and fast method for fabricating functional plasmonic devices and components [17–20,38,39]. The substrate used for sample fabrication is a standard microscopy glass cover slide of 150 μm thickness coated with a 50 nm layer of gold. The SP-ARROW structures, according to the scheme given in Fig. 1, are written into commercial negative-tone UV lithographic resist mr-NIL 6000.5 (microresist technology GmbH), which is spin-coated onto the surface of the gold film. This photoresist is well-suited for the fabrication of plasmonic waveguide components, both by 2PP laser direct-writing [17,19] as well as nanoimprint lithography [38,39]. By spin-coating at 3000 rpm, a polymer film thickness of 500 nm is achieved. The structures are written using a frequency-doubled Yb:glass laser, working at a wavelength of 522 nm with a repetition rate of 1 MHz [18]. The femtosecond laser pulses are focused by an immersion-oil objective (Zeiss, 100× magnification, 1.4 NA). Further details of the fabrication process of dielectric ridges forming the bandgap structure are described elsewhere [17,19].

As already described above, the bandgap-confined SPP waveguide consists of a narrow region of 7 μm width between two dielectric ridges on top of the gold film. The width and height of the ridges are 650 and 500 nm, respectively. The Bragg reflector is formed by their inner and outer sidewalls. This waveguide is investigated at 1550 and 974 nm (vacuum wavelength), since cheap diode laser sources are easily available at these wavelengths. For the given structural parameters, the waveguide is single mode for the wavelength around 1550 nm, and it supports two modes at 974 nm.

For local excitation of the waveguide modes, an additional ridge with the same cross-sectional parameters is added at one side of the waveguide perpendicular to the waveguide axis, in the following referred to as the “coupling ridge.” To increase the confinement of the SPP modes to the waveguide core, one or two further polymer ridges can be added on each side with a separation of about 1.5 μm.

B. Characterization of Photonic Bandgap-Confined SPP Waveguides

The excitation and propagation of SPPs are investigated by imaging the SPP leakage radiation, which is emitted from the gold–glass interface by LRM. LRM is a dynamic technique offering the capability for fast visualization of SPPs and their interaction. These features have made it a popular method to study the behavior of SPPs in a broad variety of experiments in the visible and infrared wavelength regions [18].

SPPs are locally excited using continuous-wave laser diodes working at wavelengths of 1550 and 974 nm, respectively, as well as a titanium sapphire laser working at 775 nm. The laser radiation is focused by a 40× objective

onto the coupling ridge of the plasmonic waveguide. Due to scattering on the ridge with subwavelength dimensions, the light can couple to propagating SPP modes in the waveguide, which subsequently couple again to propagating modes in the glass substrate, i.e., the leakage radiation being emitted by the SPPs. This leakage radiation is collected by a 100× immersion-oil objective, as it has also been used for the structure fabrication. For the visualization of the infrared radiation at 1550, 974, and 775 nm, InGaAs and Si-CMOS cameras are used. As an example, LRM images at 1550 nm together with optical microscope images of the bandgap-confined SPP waveguides are shown in Fig. 4.

In contrast to a conventional microscope setup, the tube lens is shifted to twice its nominal distance from the microscope objective to provide an image of the back focal plane before imaging onto a camera. A description of the Fourier image analysis used here can be found, for example, in [23]. Both the direct image of the metal surface and the back focal plane are recorded for investigations of the guiding properties of the waveguides. In the back focal plane, the radiation emitted from the substrate is separated by emission angles with respect to the surface normal, enabling the distinction between scattered light, SPP modes on the metal surface, and SPP modes of the waveguide structure. In this respect, this plane is also termed Fourier plane and allows the mode refractive index to be measured.

4. RESULTS AND DISCUSSIONS

In this study, bandgap SPP waveguides with one, two, and three confining dielectric ridges are investigated. The waveguide parameters, as described above, are chosen on the basis of previous numerical calculations [35]. Distributions of the fundamental mode intensity for an excitation wavelength of 1550 nm along the core regions of the corresponding waveguides with one, two, and three ridges are presented in Fig. 4. The electromagnetic energy is concentrated basically in the center of the waveguide in the core region, demonstrating its good collimation. Measurements of the SPP intensity along the waveguide axis by LRM show a propagation length in all three structures of about 41 μm [see Fig. 5(a)]. The intensity decay is fitted by an exponential curve with the same decay length.

Since the effective index of the waveguide mode is different from the optical and SPP modes in the ridges, only a weak coupling of energy to the ridges occurs [35]. Still, a small portion of SPPs could leak through the confining structure. In principle, it is possible to reduce this leakage by increasing the number of ridges in the system. However, this effect is small, and the propagation length shows only weak dependence on the number of confining ridges in the Bragg reflectors.

The measured propagation length is shorter compared to the numerical simulations, which is attributed to the fact that the leakage radiation introduces additional losses to the SPP propagation. This effect is not included in the FEM simulations because their results only provide the properties of

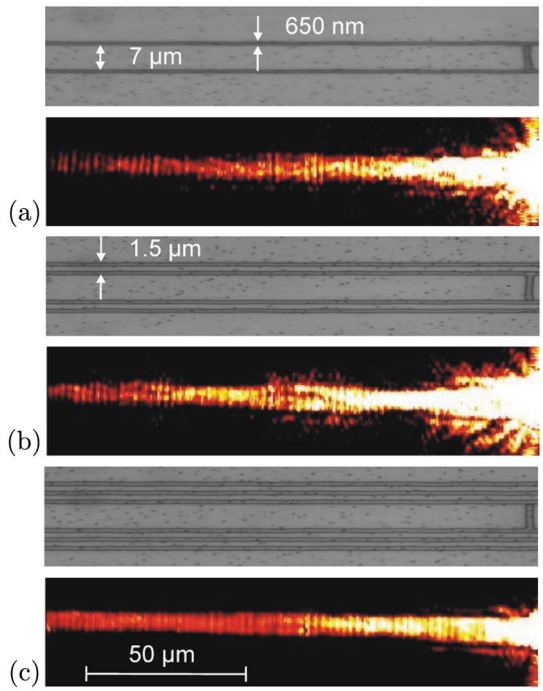

Fig. 4. Optical microscope images of the waveguide structures together with corresponding LRM images of the fundamental SPP mode for an excitation wavelength of 1550 nm. (a) SPPBG structure with one ridge per side of the waveguide. (b) Two ridges per side. (c) Three ridges per side. The width of the confining ridges is 650 nm with a height of 500 nm. The ridges are separated by 1.5 μm on each side and confine a guiding region of 7 μm width.

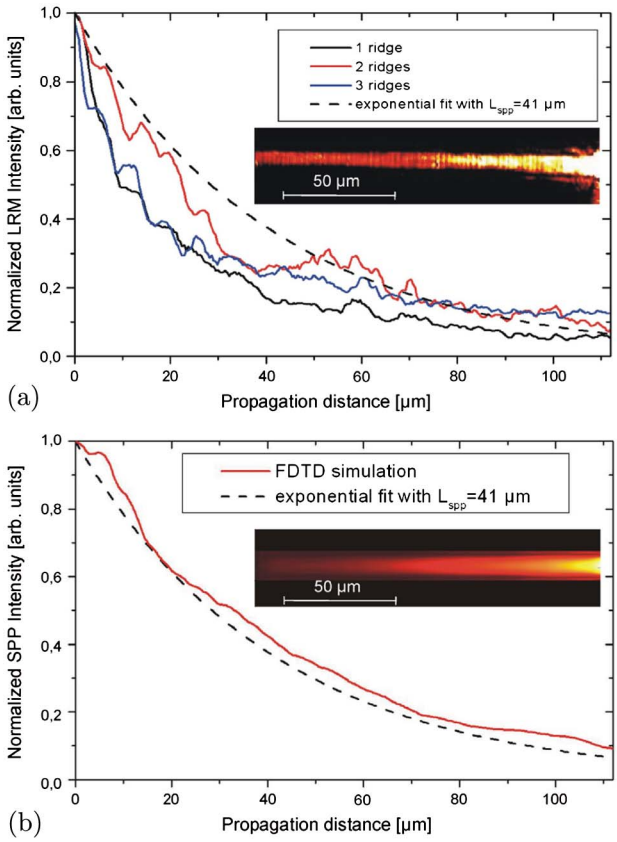

Fig. 5. (a) SPP propagation lengths at 1550 nm measured by LRM for waveguide with one, two, and three ridges per side. (b) Propagation length of the SPP electric-field intensity obtained from FDTD simulation. Both results are compared with an exponential curve with a decay length of 41 μm showing good agreement with experimental and numerical results. The insets show the LRM image and FDTD simulation, respectively.

distinct eigenmodes, but not the coupling between them. In the present case, the coupling of SP-ARROW eigenmodes to the radiation modes in the glass substrate must be taken into account. In order to demonstrate that this coupling is indeed responsible for the reduced propagation length and that correct propagation length can be obtained when taking this into account, additional FDTD simulations have been performed. Details of the numerical procedure can be found in [40–42]. The propagation length obtained from the FDTD simulation shown in Fig. 5(b), taking into account the SP-ARROW structure, the gold film, and the glass substrate, matches well with the measured length of 41 μm. The obvious deviations from the pure exponential decay are due to the weak coupling of the SP-ARROW mode to optical and plasmonic modes inside and between the ridges.

With decreasing wavelength, the electromagnetic field distribution in the system can change significantly [35]. In the wavelength range between 1300 and 1400 nm, propagation constants of modes inside the dielectric ridges can overlap with the waveguide mode, and electromagnetic power can be concentrated basically inside the ridges. For further decreasing wavelength, the waveguide again can support propagation of SPP modes, but in that case the structure appears to support two or more modes. For an excitation wavelength of 974 nm, two modes are found according to the FEM simulations in agreement with the leakage radiation investigations. Their excitation depends on the focusing conditions of the incident laser beam. Figure 6 demonstrates the simultaneous propagation of the SPP modes for excitation with a single beam at a wavelength of 974 nm focused to a spot size of approximately 2 μm. The leakage radiation images are shown in Fig. 6(a) (middle image) together with a microscopic image of the structure and results of FDTD simulation (upper and lower images, respectively). In comparison with the leakage radiation images in Fig. 4 for an excitation wavelength of 1550 nm, leakage radiation here is also visible between the ridges in the reflectors in correspondence to the FEM simulations of the mode structure in Fig. 3.

The small difference between propagation constants of the modes results in a complex beating pattern of the intensity distribution in Fig. 6(a) along the waveguide axis, where the plasmonic energy oscillates between the two modes. A typical Fourier plane image of the SPP intensity distribution is shown in Fig. 6(b). Although the resolution in the Fourier image is not sufficient to fully resolve the two modes, a slight difference in effective mode indices is still visible. The signatures corresponding to the fundamental and the first higher mode are indicated by the arrows in Fig. 6(b). In addition, signatures of SPPs propagating into the opposite direction of the excitation ridge onto the plane metal surface are visible, though the SPPs are not shown in the LRM images. By inspection of the Fourier image, the confined waveguide SPP modes indicate an effective index slightly lower than 1.01 in good correlation with the FEM results for the mode indices. The propagation of the two SPP modes in the waveguide is visible over the whole 125 μm wide image. However, due to the simultaneous excitation of two modes in the SP-ARROW and their complex intensity distribution, exact values for the mode propagation length cannot be given.

In order to determine the mode propagation length, different modes have to be excited selectively. Using just one beam

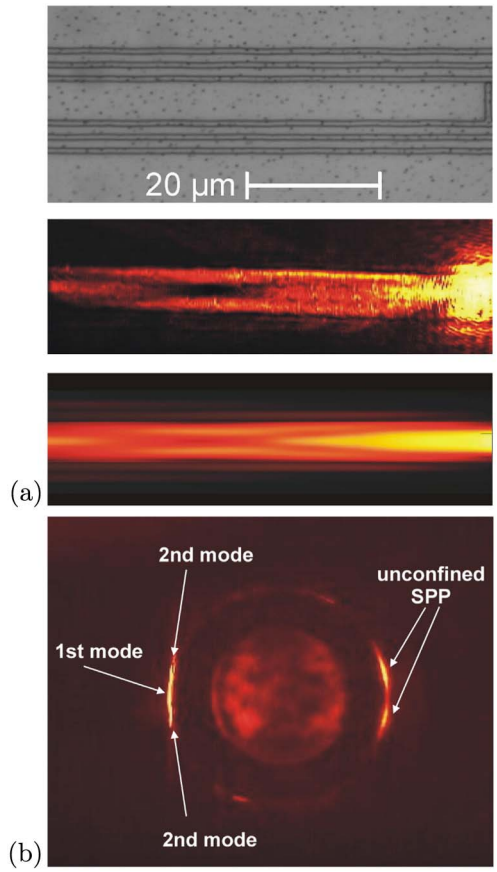

Fig. 6. (a) From top to bottom: optical microscope image, corresponding leakage radiation image, and FDTD simulation of the SPP electric-field intensity, showing a redistribution of energy from the center to the outer waveguide region and back. The excitation wavelength is 974 nm. (b) Image of the leakage radiation in the Fourier (back focal) plane. Arrows indicate the signatures of first and a weak contribution of the second SPP mode. The nonconfined SPPs propagating to the right are not shown in the LRM images.

at 974 nm, it is hard to excite only one waveguide mode, which is partly due to the multimode beam profile of the laser diode. Nonetheless, selective excitation of the two modes in the system can be realized by SPP excitation with two coherent laser beams with an adjustable phase delay. The two phase-coupled laser beams are realized by a Michelson interferometer and focused next to each other onto the coupling ridge, as demonstrated in Fig. 7. Two laser beams at 974 nm with zero (modulo 2π) phase difference (in-phase) irradiating the coupling ridge lead to the excitation of only the fundamental mode [Fig. 7(a)] with an intensity maximum on the waveguide axis. The propagation length can be measured from the LRM image to approximately 43 μm. If the two beams have a phase difference of π (out-of-phase), only the higher SPP waveguide mode is excited and appears as two bright stripes along the outer core regions [Fig. 7(b)]. In this case, fields in the two intensity maxima of the waveguide have opposite signs in correspondence with the out-of-phase laser beams. The decay length of this mode is 47 μm and is slightly longer than that for the fundamental mode. In the Fourier plane images shown in Fig. 7, the different modes are indicated by arrows. The bright straight lines tangent to the circular signature of SPPs on the plane metal surface exhibit either a maximum at the tangent point (in-phase) or a minimum (out-of-phase)

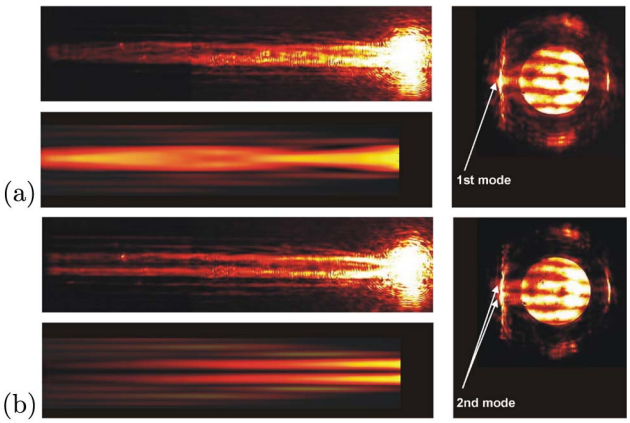

Fig. 7. (a) Leakage radiation: experiment and FDTD simulation (left position) and Fourier plane images (right position) of the fundamental SPP mode in the waveguide selectively excited by two in-phase laser beams. (b) Leakage radiation: experiment and FDTD simulation (left position), and Fourier plane images (right position) of the second SPP mode in the waveguide selectively excited by two out-of-phase laser beams. Excitation wavelength is 974 nm. The arrows indicate the position of the Fourier images of the first (fundamental) and second SPP modes.

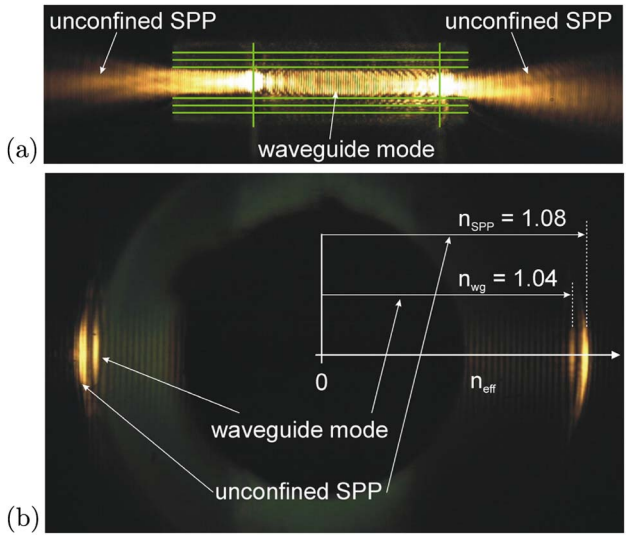

Fig. 8. Interference pattern of two counterpropagating waveguide modes excited at a wavelength of 775 nm. The SP-ARROW contains an additional layer of polymer with the refractive index of 1.5 and height of 32 nm. The interference pattern can be used for sensing changes in the refractive index of the medium above the metal film surface. (a) The image plane with the waveguide modes and the unconfined SPPs propagation away from the waveguide. (b) The corresponding Fourier image indicating the effective waveguide mode index of 1.04, whereas the effective index of the unconfined SPP is 1.08.

corresponding to the excitation of the fundamental [Fig. 7(a)] and second [Fig. 7(b)] modes. The ability to adjust the phase of the individual laser pulses gives the possibility to coherently control the mode excitation process.

5. DEMONSTRATION OF SENSING PROPERTIES

The SP-ARROW opens further possibilities for the realization of compact and integrated sensing elements by measuring changes in the effective mode indices. As a first and simple example, the influence of a thin polymer layer on the propagation of unconfined SPPs and bandgap-confined SPP waveguide modes shall be demonstrated. The development of a complete sensor element is beyond the scope of this paper and only the principal possibilities shall be outlined in this section.

In this experiment, the SPPs and waveguide modes are excited at a wavelength of $\lambda = 775$ nm using a Ti:sapphire laser. This laser source has been chosen due to its good beam profile and the possibility to use a higher resolution Si-CMOS camera (1280×1024 pixel). Although the waveguide is multimode, the good laser-beam profile combined with weak focusing (focus diameter 5 μm) allows excitation of only the fundamental mode. The waveguide modes excited at opposite ends of the SP-ARROW form an interference pattern inside the waveguide, see Fig. 8(a). This interference pattern is not of concern for the following consideration. The waveguide is excited at both ends to have a direct comparison of the effective indices of free SPPs and waveguide modes, with the signatures now being visible on the same side of the Fourier plane image in Fig. 8(b).

First, the mode effective indices are determined for the system without an additional polymer layer. The effective indices of the fundamental waveguide mode with air as the supertrate is determined by FEM to $n_{wg}^0 = 1.007$, a measurement of the mode index by LRM, as described above, reveals $n_{wg}^0 = 1.01$. The effective index of the unconfined SPPs on the metal film is measured to $n_{\mathrm{SPP}}^0 = 1.02$. This value is in correspondence with $n_{\mathrm{SPP}}^0 = 1.021$ obtained by evaluating the reflection minimum of the Fresnel reflection coefficients for p-polarized light for the three-layer system [glass–50 nm gold—air] using the transfer matrix method (TMM). The observed difference in the refractive indices, inside and outside the ARROW structure, is attributed to the difference in distributions of guided and unguided electromagnetic fields.

If now an additional thin layer of polymer with a refractive index of 1.5 is deposited onto the sample containing the SP-ARROW structure, the effective indices of the unconfined SPPs and the guided surface plasmons change. The thickness of the additional layer is determined by measuring the effective refractive index of the free propagating SPP and comparing this result to the theoretical description based on the TMM. From Fig. 8(b), one measures for the unconfined SPP an effective index of $n_{\mathrm{SPP}} = 1.08$. The present layer thickness is now determined by matching this result to the Fresnel reflection minimum from a four-layer system [glass–50 nm gold–X nm polymer–air] by the TMM. The comparison to the experimental data gives a polymer layer thickness of $X = 32$ nm.

Now the confined SPP mode is considered. The effective mode index of the fundamental SP-ARROW mode is measured from Fig. 8(b) to $n_{wg} = 1.04$. Taking into account the polymer layer and using the measured layer thickness of $X = 32$ nm, the FEM simulation of the mode effective index for the given experimental configuration results in an effective mode index for the fundamental mode of $n_{wg} = 1.045$, which is in good agreement with measurements. For the 32 nm thick polymer layer, a clear shift of the effective index compared to the case of air as a superstrate is observed, both theoretically and experimentally. With the present resolution of the optical imaging system, a minimal refractive index shift of 0.003 can be

observed, corresponding to a polymer layer with a bulk refractive index of 1.5 of 5 nm. This sensitivity is comparable to those published in [43].

To achieve higher resolutions and to exploit the sensing properties of plasmonic ARROWs, the combination of long propagation lengths together with the possibility to use fiber in- and outcoupling is suggested. When the gold layer is sufficiently thick to suppress emission of leakage radiation, the propagation length increases above the values measured in the previous experiments. If the waveguide mode is outcoupled into a fiber after a total propagation length of $L = 200$ μm, the signal can be interfered with a reference signal. During its propagation, the SPP acquires a phase shift that causes a change in signal intensity. If we assume an effective mode index difference of $\Delta n = 0.0001$ rad, which is the difference between air and carbon dioxide as superstrate, it would lead to a phase shift of $\Delta\phi = 2 * \pi/\lambda * L * \Delta n = 0.16$ rad. This phase difference shall result in a clearly visible change in interferometric signal intensity. These possibilities might open new ways for realizing highly sensitive and compact sensor elements.

6. CONCLUSION

The optical properties of large mode-area bandgap-confined antiresonant-reflecting optical waveguides for surface plasmon-polaritons (SP-ARROWs) have been experimentally investigated. The experimental results have been supported by numerical FEM and FDTD simulations. These novel types of SPP waveguides have been fabricated using the fast and cost-effective method of 2PP. Optical characterization of the guiding properties for SPPs has been performed by LRM for excitation wavelengths of 974 and 1550 nm. At the telecommunication wavelength at 1550 nm, single-mode operation is observed, and a propagation length of 41 μm has been measured. The propagation length is limited by the losses imposed by the leakage radiation, as has been confirmed by comparison of the experimental results with FDTD simulations. Longer propagation lengths of more than 100 μm, as obtained from FEM simulations, can be reached using thicker gold films to suppress the leakage radiation. For excitation of the SP-ARROW with 974 nm, selective excitation of the fundamental and the first higher-order plasmonic mode has been demonstrated using two coherent phase-coupled laser beams, allowing the propagation lengths of these modes to be measured individually to 43 and 47 μm, respectively. For both excitation wavelengths, the single-mode regime with large mode field diameters of about 5 μm provide the possibility to efficiently couple these types of SPP waveguides to optical fibers. Further possibilities for sensing applications of the proposed and characterized waveguide structure have been demonstrated. As a first example, the influence of a thin polymer layer on top of the waveguide on the confined and unconfined propagation constants has been quantified using an excitation wavelength of 775 nm. The experimental measurements of the effective mode indices and the polymer layer thickness show good agreement with theoretical and numerical simulations. For future applications, the combination of long propagation lengths in plasmonic ARROWs together with the possibility to use fiber in- and outcoupling opens new ways for realizing highly sensitive and compact sensors.

ACKNOWLEDGMENTS

The authors acknowledge financial support of this work by the Schwerpunktprogramm SPP1391 “Ultrafast Nanooptics” of the Deutsche Forschungsgemeinschaft (DFG), the VolkswagenStiftung within the project “Nanostrukturierte Polymere für Anwendungen in der Optik/Nanostructured Polymers for Applications in Optics,” and the Collaborative Research Center/Transregio 123 “Planar Optronic Systems of the German Research Foundation (Deutsche Forschungsgemeinschaft, DFG). The authors further acknowledge support by the Center for Quantum Engineering and Space-Time Research (QUEST), and the Laboratory of Nano- and Quantum Engineering (LNQE) of the Leibniz University Hannover.

REFERENCES

1. A. V. Zayats, I. I. Smolyaninov, and A. A. Maradudin, “Nano-optics of surface plasmon polaritons,” Phys. Rep. **408**, 131–314 (2005).
2. S. A. Maier, *Plasmonics-Fundamentals and Applications* (Springer, 2007).
3. M. L. Brongersma and P. G. Kik, *Surface Plasmon Nanophotonics* (Springer, 2007).
4. H. Ditlbacher, J. R. Krenn, G. Schider, A. Leitner, and F. R. Aussenegg, “Two-dimensional optics with surface plasmon polaritons,” Appl. Phys. Lett. **81**, 1762–1764 (2002).
5. J. R. Krenn, H. Ditlbacher, G. Schider, A. Hohenau, A. Leitner, and F. R. Aussenegg, “Surface plasmon micro- and nano-optics,” J. Microsc. **209**, 167–172 (2003).
6. A. L. Stepanov, J. R. Krenn, H. Ditlbacher, A. Hohenau, A. Drezet, B. Steinberger, A. Leitner, and F. R. Aussenegg, “Quantitative analysis of surface plasmon interaction with silver nanoparticles,” Opt. Lett. **30**, 1524–1526 (2005).
7. S. I. Bozhevolnyi, V. S. Volkov, E. Devaux, J.-Y. Laluet, and T. W. Ebbesen, “Channel plasmon subwavelength waveguide components including interferometers and ring resonators,” Nature **440**, 508–511 (2006).
8. I. P. Radko, S. I. Bozhevolnyi, A. B. Evlyukhin, and A. Boltasseva, “Surface plasmon polariton beam focusing with parabolic nanoparticle chains,” Opt. Express **15**, 6576–6582 (2007).
9. A. B. Evlyukhin, S. I. Bozhevolnyi, A. L. Stepanov, R. Kiyan, C. Reinhardt, S. Passinger, and B. N. Chichkov, “Focusing and directing of surface plasmon polaritons by curved chains of nanoparticles,” Opt. Express **15**, 16667–16680 (2007).
10. I. P. Radko, S. I. Bozhevolnyi, G. Brucoli, L. Martin-Moreno, F. J. Garcia-Vidal, and A. Boltasseva, “Efficient unidirectional ridge excitation of surface plasmons,” Phys. Rev. B **78**, 115115 (2008).
11. H. Liu, P. Lalanne, X. Yang, and J. P. Hugonin, “Surface plasmon generation by subwavelength isolated objects,” IEEE J. Sel. Top. Quantum Electron. **14**, 1522–1529 (2008).
12. B. Wang, L. Aigouy, E. Bourhis, J. Gierak, J. P. Hugonin, and P. Lalanne, “Efficient generation of surface plasmon by single-nanoslit illumination under highly oblique incidence,” Appl. Phys. Lett. **94**, 011114 (2009).
13. A. B. Evlyukhin, C. Reinhardt, E. Evlyukhina, and B. N. Chichkov, “Asymmetric and symmetric local surface-plasmon-polariton excitation on chains of nanoparticles,” Opt. Lett. **34**, 2237–2239 (2009).
14. S. I. Bozhevolnyi and J. Jung, “Scaling for gap plasmon based waveguides,” Opt. Express **16**, 2676–2684 (2008).
15. E. Verhagen, J. A. Dionne, L. Kuipers, H. A. Atwater, and A. Polman, “Near-field visualization of strongly confined surface plasmon polaritons in metal-insulator-metal waveguides,” Nano Lett. **8**, 2925–2929 (2008).
16. E. Verhagen, M. Spasenovic, A. Polman, and L. Kuipers, “Nanowire plasmon excitation by adiabatic mode transformation,” Phys. Rev. Lett. **102**, 203904 (2009).
17. A. Seidel, C. Reinhardt, T. Holmgaard, W. Cheng, T. Rosenzveig, K. Leosson, S. I. Bozhevolnyi, and B. N. Chichkov, “Demonstration of laser-fabricated DLSPPW at telecom wavelength,” IEEE Photon. J. **2**, 652–658 (2010).

18. C. Reinhardt, A. Seidel, A. B. Evlyukhin, W. Cheng, R. Kiyan, and B. N. Chichkov, "Direct laser-writing of dielectric-loaded surface plasmon-polariton waveguides for the visible and near infrared," Appl. Phys. A **100**, 347–352 (2010).
19. C. Reinhardt, S. Passinger, B. N. Chichkov, C. Marquart, I. P. Radko, and S. I. Bozhevolnyi, "Laser-fabricated dielectric optical components for surface plasmon polaritons," Opt. Lett. **31**, 1307–1309 (2006).
20. R. Kiyan, C. Reinhardt, S. Passinger, A. L. Stepanov, A. Hohenau, J. R. Krenn, and B. N. Chichkov, "Rapid prototyping of optical components for surface plasmon polaritons," Opt. Express **15**, 4205–4215 (2007).
21. J. Grandidier, S. Massenot, G. Colas des Francs, A. Bouhelier, J.-C. Weeber, L. Markey, A. Dereux, J. Renger, M. U. González, and R. Quidant, "Dielectric-loaded surface plasmon polariton waveguides: figures of merit and mode characterization by image and Fourier plane leakage microscopy," Phys. Rev. B **78**, 245419 (2008).
22. S. Massenot, J. Grandidier, A. Bouhelier, G. Colas des Francs, L. Markey, J.-C. Weeber, A. Dereux, J. Renger, M. U. Gonzàlez, and R. Quidant, "Polymer-metal waveguides characterization by Fourier plane leakage radiation microscopy," Appl. Phys. Lett. **91**, 243102 (2007).
23. C. Reinhardt, A. Seidel, A. B. Evlyukhin, W. Cheng, and B. N. Chichkov, "Mode-selective excitation of laser-written dielectric-loaded surface plasmon polariton waveguides," J. Opt. Soc. Am. B **26**, B55–B60 (2009).
24. C. Reinhardt, R. Kiyan, S. Passinger, A. L. Stepanov, A. Ostendorf, and B. N. Chichkov, "Rapid laser prototyping of plasmonic components," Appl. Phys. A **89**, 321–325 (2007).
25. P. Berini, R. Charbonneau, and N. Lahoud, "Long-range surface plasmons on ultrathin membranes," Nano Lett. **7**, 1376–1380 (2007).
26. P. Berini, "Long-range surface plasmon-polaritons," Adv. Opt. Photon. **1**, 484–588 (2009).
27. A. B. Evlyukhin and S. I. Bozhevolnyi, "Surface plasmon polariton guiding by chains of nanoparticles," Laser Phys. Lett. **3**, 396–400 (2006).
28. D. Van Orden, Y. Fainman, and V. Lomakin, "Optical waves on nanoparticle chains coupled with surfaces," Opt. Lett. **34**, 422–424 (2009).
29. S. I. Bozhevolnyi, J. Erland, K. Leosson, P. M. W. Skovgaard, and J. M. Hvam, "Waveguiding in surface plasmon polariton band gap structures," Phys. Rev. Lett. **86**, 3008–3011 (2001).
30. T. Søndergaard and S. I. Bozhevolnyi, "Vectorial model for multiple scattering by surface nanoparticles via surface polariton-to-polariton interactions," Phys. Rev. B **67**, 165405 (2003).
31. I. P. Radko, V. S. Volkov, J. Beermann, A. B. Evlyukhin, T. Søndergaard, A. Boltasseva, and S. I. Bozhevolnyi, "Plasmonic metasurfaces for waveguiding and field enhancement," Laser Photon. Rev. **3**, 575–590 (2009).
32. H. A. Jamid and M. N. Akram, "Analysis of antiresonant reflecting optical waveguide gratings by use of the method of lines," Appl. Opt. **42**, 3488–3494 (2003).
33. M. A. Duguay, Y. Kokubun, T. L. Koch, and L. Pfeiffer, "Antiresonant reflecting optical waveguides in SiO2-Si multilayer structures," Appl. Phys. Lett. **49**, 13–15 (1986).
34. L. J. Mawst, "High-power single-mode antiresonant reflecting optical waveguide-type diode lasers," Proc. SPIE **2382**, 155–164 (1995).
35. A. Markov, C. Reinhardt, B. Ung, A. B. Evlyukhin, W. Cheng, B. N. Chichkov, and M. Skorobogatiy, "Photonic bandgap plasmonic waveguides," Opt. Lett. **36**, 2468–2470 (2011).
36. http://www.rsoftdesign.com/.
37. V. Ferreras Paz, M. Emons, K. Obata, A. Ovsianikov, S. Peterhaensel, K. Frenner, C. Reinhardt, B. N. Chichkov, U. Morgner, and W. Osten, "Development of functional sub-100 nm structures with 3D two-photon polymerization technique and optical methods for characterization," J. Laser Appl. **24**, 042004 (2012).
38. A. Seidel, J. Gosciniak, M. U. Gonzalez, J. Renger, C. Reinhardt, R. Kiyan, R. Quidant, S. I. Bozhevolnyi, and B. N. Chichkov, "Fiber-coupled surface plasmon polariton excitation in imprinted dielectric-loaded waveguides," Int. J. Opt. Comput. **2010**, 897829 (2010).
39. A. Seidel, C. Ohrt, S. Passinger, C. Reinhardt, R. Kiyan, and B. N. Chichkov, "Nanoimprinting of dielectric loaded surface plasmon-polariton waveguides from masters fabricated by 2-photon polymerization technique," J. Opt. Soc. Am. B **26**, 810–812 (2009).
40. S. Passinger, A. Seidel, C. Ohrt, C. Reinhardt, A. L. Stepanov, R. Kiyan, and B. N. Chichkov, "Novel efficient design of Y-splitter for surface plasmon polariton applications," Opt. Express **16**, 14369–14379 (2008).
41. A. Zukauskas, M. Malinauskas, C. Reinhardt, B. N. Chichkov, and R. Gadonas, "Closely packed hexagonal conical microlens array fabricated by direct laser photopolymerization," Appl. Opt. **51**, 4995–5003 (2012).
42. C. Lemke, C. Schneider, T. Leissner, D. Bayer, J. W. Radke, A. Fischer, P. Melchior, A. B. Evlyukhin, B. N. Chichkov, C. Reinhardt, M. Bauer, and M. Aeschlimann, "Spatiotemporal characterization of SPP pulse propagation in two-dimensional plasmonic focusing devices," Nano Lett. **13**, 1053–1058 (2013).
43. M. Mrksich, G. B. Sigal, and G. M. Whitesides, "Surface plasmon resonance permits in situ measurement of protein adsorption on self-assembled monolayers of alkanethiolates on gold," Langmuir **11**, 4383–4385 (1995).